A Search for Bound Θ^+ Nuclei in Hall A

A New Proposal to Jefferson Lab PAC27

E. Chudakov, R. J. Feuerbach (spokesperson),
J. O. Hansen, J. J. LeRose, B. Wojtsekhowski
Thomas Jefferson National Accelerator Facility, Newport News, VA 23606

P. E. Reimer
Argonne National Laboratory, Argonne, IL 60439

D. J. Margaziotis
California State University, Los Angeles, CA 90032

P. Markowitz (co-spokesperson)
Florida International University, Miami, FL 33199

O. Gayou
Massachusetts Institute of Technology, Cambridge, MA 02139

K. Paschke
University of Massachusetts, Amherst, MA 01003

A. J. Sarty
St. Mary's University, Halifax, Nova Scotia CANADA B3H 3C3

J. R. Calarco
University of New Hampshire, Durham, NH 03824

December 6, 2004

Abstract

We propose to search for bound Θ^+-hyponuclear states, opening a new field of multi-body spectroscopy. The energy of the bound states would be measured with 1 MeV accuracy, lending information about the effective potential well and therefore the Θ^+-nucleon and Θ^+-meson interactions. Various quark-model calculations will also benefit from the different arrangement of quarks within the Θ^+, making it differently-sensitive to the quark-meson couplings. Multiple predictions have been made for the existence of Θ^+-hyponuclei, and tend to find an attractive potential depth of at least 50 MeV. While not all the models predict binding energies large enough to prevent the Θ^+ from decaying strongly, its narrow width and those of the nuclear states are expected to permit the measurement of at least the first several energy levels.

The reaction under study is $^{12}C(e,e'K^-)^{12}_{\Theta}C$, where the medium-size ^{12}C nucleus is light enough to have only a handful of nucleon and Θ^+ single particle states to contribute, and heavy enough to bind the pentaquark. This high-luminosity experiment will utilize existing Hall A equipment and detectors. The HRS's in conjunction with the septum magnets will be used to detect the scattered electron and outgoing K^- at an angle $\pm 6^\circ$ with respect to the beam to both maximize the virtual photon flux and minimize the momentum transfer to the target nucleus. We request 200hrs of beamtime in order to be sensitive at the 6σ level for a Θ^+ total photo-production cross-section $\sigma_{\gamma n}$ of 10 nb.

1 Introduction

Recently there has been a flurry of excitement at the discovery[1] of a new exotic baryonic state with $S = +1$. Denoted as the Θ^+, it has been observed subsequently in multiple independent experiments[2, 3, 4, 5, 6, 7]. Due to its positive strangeness and decay through the K^+n and K^0p channels, its minimal quark configuration is that of a five-quark (pentaquark) $uudd\bar{s}$ state. While such a state was predicted in a chiral soliton model as a member of an antidecuplet of the flavor group $SU(3)_F$[8], the spin, isospin, and parity of the Θ^+ are unknown. Beyond its positive strangeness, the Θ^+ is also remarkably narrow, with direct observations limiting its width to 15 MeV due to experimental resolution. An indirect measurement through the re-analysis of data taken with a kaon beam suggests the Θ^+'s width is of order 1 MeV or less[9].

Though it has been observed in multiple low and moderate energy experiments, the measurements have had the same moderate statistical significance, showing up as a several-σ fluctuation above a complex background. Searches have been conducted at high-energy, high-luminosity accelerator facilities, but with a negative result where naively, based upon the lower luminosity experiments, the Θ^+ should have been very evident; while the discrepancy can be explained[10], the community is unsettled by the lack of a high-statistics observation and measurement of the state. To clarify the matter, both SPring-8 and CLAS collected two to ten-times larger datasets in 2004, with the results of the analyses highly anticipated and expect by early 2005.

The spin, parity, and isospin of the pentaquark state are unknown, and are an active area of theoretical debate and discussion. The chiral-soliton model [8] that motivated the search for the Θ^+ predicts it to be an $I = 0, J^P = \frac{1}{2}^+$ state, as does the diquark model[11] and many other models with very different inputs. Constituent quark model prefer a negative parity for the exotic baryon, while lattice-gauge calculations are generating mixed results[12]. A challenge confronting models which favor a positive-parity state is to explain the Θ^+'s low mass, since conventionally the necessary unit of angular momentum would increase the particle's mass by 600 MeV[13]. A definitive statement about the parity of the Θ^+ would have a significant impact as to the understanding of its internal structure.

One approach that has not yet been utilized to study the Θ^+ is to exploit its interactions within nuclei. Such a measurement would be sensitive to the Θ^+'s meson and nucleon couplings differently from the 'free-production' observations made so far. Specifically, the greater number of u and d quarks inside the Θ^+ give it a different sensitivity to the quark-meson coupling constants used in relativistic mean-field and quark mean-field theory models[14, 15]. Recently multiple calculations utilizing different approaches have concluded that the Θ^+, assuming it has positive parity, should be able to form a bound state within nuclei[13, 14, 15, 16, 17]. Taken together, the calculations conclude:

- the decay width of the Θ^+ should be narrower within the nucleus than in free space, by perhaps a factor of three[14, 15, 16, 17];
- the depth of the potential is of order 50-120 MeV or more;
- and the energy levels of the bound states would be separated by 10-20 MeV, narrower than the expected width of the Θ^+ [14, 15, 16].

These predictions invite the study of the Θ^+ inside nuclei, analogous to the measurements of Λ-hypernuclei that has been carried out over the past several decades. In the instance where the Θ^+ has negative-parity, a chiral soliton model[17] calculation found the pentaquark's nuclear binding energies to be between 5 and 86 MeV greater than that of a nucleon, depending upon the variation of the model. So, for both a positive and negative parity Θ^+, there is strong reason to expect the Θ^+ to form bound nuclear states.

We therefore propose a search for Θ^+-hyponuclei with the $^{12}C(e, e'K^-)^{12}_{\Theta}C$ reaction in Hall A utilizing its high luminosity capabilities, ability to detect particles at small angles, and its excellent momentum and angular resolutions. The basic approach is similar to the recently run and successful E94-107 Hall A experiment[18], though with modifications to account for the higher particle-flux into the K^- arm and the subsequent higher coincidence rate.

The proposal is organized as follows. In section 2 a brief review of the current understanding of the Θ^+ and Θ^+-hyponuclei is presented. Section 3 describes the general layout of the experiment. In section 4 we go into detail about the experimental apparatus and conditions, namely the detectors and expected non-signal rates. The expected $^{12}_{\Theta}C$-excitation spectra and the beam-time request are presented in section 5. Finally, we summarize the expected results and make the beam-time request in section 6.

2 Motivation

2.1 Theoretical status

The idea for searching for Θ^+-hyponuclei originated with a schematic model created in an attempt to find a reason for the Θ^+'s light mass and small width[13]. In the framework of the quark model, a large residual interaction is required to lower the mass of the Θ^+ to the experimentally observed value of 1540 MeV. Since such a large effect cannot be expected to arise from QCD, the additional strength must come from collective effects. By describing the Θ^+ as a coherent set of color-single $d\bar{s}$,$u\bar{s}$ pseudoscaler excitations in a p-wave relative to the nucleon, the attraction between the excitations and the nucleon can remain modest yet the mass, width and K^* coupling to the Θ^+ can be accounted for. The overall effect is similar to the mechanism used to describe the nuclear giant dipole resonance. The result of this collective action is a strong attractive potential for the Θ^+, with a depth on the order of 200-400 MeV. Since the threshold energy of the Θ^+ is 107 MeV ($M_\Theta^+ - M_N - M_K = 107$MeV), a pentaquark bound by more than this could only decay weakly, and could be observed in a straight-forward $A(\gamma, K^-)_{\Theta^+}B$ or $A(K^+,\pi^+)_{\Theta^+}B$ measurement, devoid of physics-background. This argument only works within the model in the case the Θ^+ has positive parity; a negative parity Θ^+ might also be bound, but with a much weaker potential.

Since then, a number of other models have been constructed, which find the Θ^+ with bound nuclear states, especially in light-to-medium nuclei[16, 14, 15, 17]. The models agree that the width of the Θ^+ in the nuclear medium should be significantly narrower than in vacuum, due in part to partial Pauli-blocking of the daughter nucleon and the reduced available energy, such that the width in-medium can be expected to be 6 MeV or less, with a preference for less than 1 MeV. The widths of the nuclear-states are also expected to be narrow. A calculation studying the self-energy of the Θ^+ found that while the ΘNK interaction was not sufficient to bind the state[19], the two-meson cloud attached to the Θ^+ (with assumptions) could generate an attractive potential with a depth of magnitude 50-120 MeV[16]. While this is not sufficient to make the Θ^+ stable against strong decays like the Λ in hypernuclei, the narrow width of the Θ^+ and the nuclear state wiould permit the study of the effective Θ^+-hyponuclei.

A quark mean-field (QMF) calculation[14] and relativistic mean-field (RMF) calculation [15], which have both been successful in describing Λ-hypernuclei, both find potential depths consistent with the self-energy result for a Θ^+ with $J^P = \frac{1}{2}^+$. Using a completely different approach, these calculations also demonstrate how sensitive the energy-levels of a Θ^+-hyponucleus are to the quark-meson coupling constants. Due to the larger number of u and d quarks within the Θ^+ as compared to within a Λ or nucleon, the weighting of the quark-meson coupling constants differs. Figure 1 shows the binding-energies from the RMF calculation; the Θ^+ binding-energies in carbon shown as (2a) and (2b) differ by several tens of MeV due to only a 5% variation of the $g^\sigma_{\Theta^+} = 4g^\sigma_{u/d}$ coupling constant. Similarly, the QMF model finds that a 3% variation of $g^\omega_{\Theta^+} = 4g^\omega_{u/d}$ leads to 10 MeV shift in the binding of the lowest energy state[14]; the same 3% variation caused only a 3 MeV correction in $_\Lambda$Ca[20]. The increased leverage due to the differ quark-mixture within the pentaquark would be a sensitive tool to measure the quark-meson couplings and improve the quark-model description of the nucleon-nucleon interaction.

In Figure 1, the binding energies from the RMF calculation are shown, with a comparison to the results from the self-energy calculation in columns (2c), (2d), (4b), and (4c). First, we note a variation of the RMF model (2b) can create a deeply bound state where the Θ^+ could decay only weakly, in agreement with Miller's hypothesis. Next, with state-widths of ≈ 6MeV or less, it would be possible to observe not only the seperation between the different orbital states, but the spin-orbit splitting between the $1p_{1/2}$ and $1p_{3/2}$ states as well. However, for maximum benefit this would require precise knowledge of the spin-orbit splitting of the nucleon hole-state as well.

The only calculation that to date accounts for a negative parity Θ^+ in nuclei is the chiral soliton calculation of Kopeliovich and Shunderuk[17]. Using a "rigid oscillator" approach, they find a wide range of possible binding energies between 97 and 178 MeV depending upon the variation of the model[1].

[1] In the chiral soliton model, the mass of the Θ^+ is greater than 1566 MeV, so even the deepest state can still undergo a strong decay.

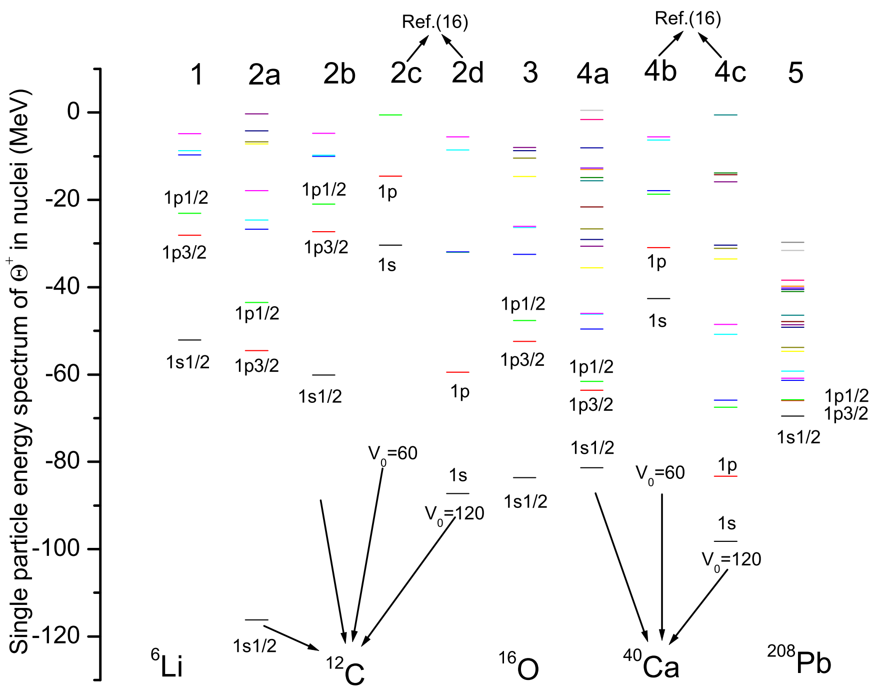

Figure 1: The single-particle levels for a Θ^+ embedded within a ^{6}Li, ^{12}C, ^{16}O, ^{40}Ca, or ^{208}Pb nucleus denoted by (1),(2a-d),(3),(4a-c), and (5), respectively. The first column for each nucleus are the results of the RMF model with a standard value of $g^{\sigma}_{\Theta} = 13.925$; column (2b) is for carbon but with $g^{\sigma}_{\Theta} = 0.95 \times 13.925$; and columns (2c,2d) and (4b,4c) are the results of the self-energy calculation in [16] at different potential depths (60 MeV,120 MeV)[15].

2.2 Experimental prospects

With a wide state separation and narrow widths, observing the different Θ^+-hyponuclear states should be straightforward were it not for a small production cross-section, necessarily large momentum transfer to produce the state, and background issues. Following up on the theoretical developments, a calculation of the $A(K^+, \pi^+)_\Theta B$ reaction was performed for a ^{12}C target[21], and a measurement of the hadronically-induced reaction is being considered to run at KEK.

3 Kinematics

A schematic of the experimental setup reaction is presented in Fig. 2. The electron scattering produces a quasi-real photon. Through diffractive processes, a $K\bar{K}$ or $K\bar{K}^*$ pair is produced. The $\bar{K}$ or $\bar{K}^*$ couples with a neutron in the ^{12}C target nucleus, producing a Θ^+. A fraction, on the order of 0.5% (discussed in 5.2), of the Θ^+ are bound within the nucleus, forming one of a handful of discrete $^{12}_{\Theta}C$ hyponuclear states. Of the $e', K, ^{12}_{\Theta}C$ three-body final-state the e' and K^- are measured directly, and the $^{12}_{\Theta}C$ is identified through the reconstructed missing-mass. Despite its strong decay, the width of the Θ^+ is expected to be narrower than the energy difference of the hyponuclear states, permitting their measurement.

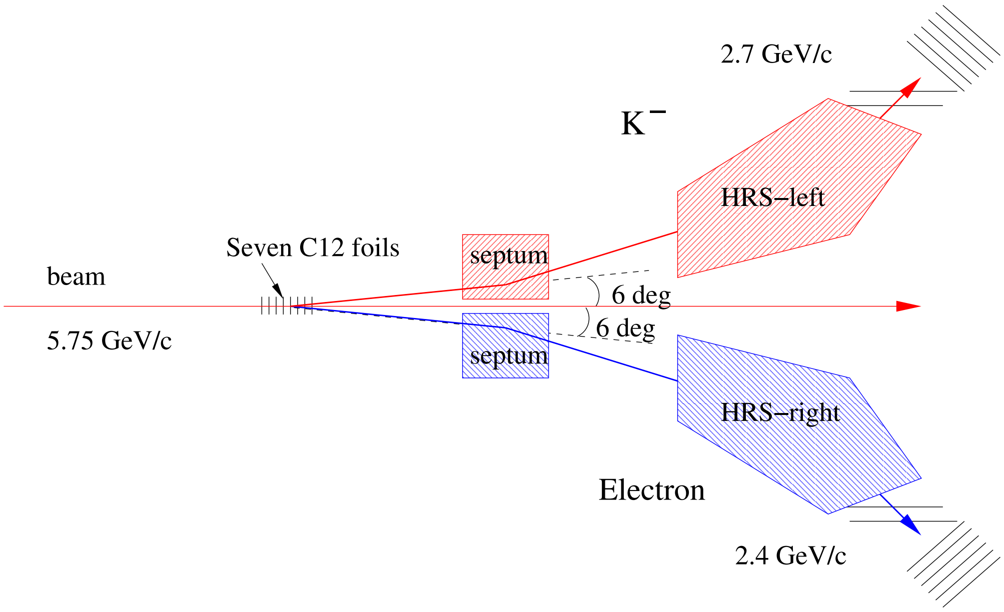

Figure 2: Experimental setup for measuring the $^{12}C(e,e'K^-)^{12}_{\Theta}C$ reaction.

A 5.75 GeV/c electron beam, with a current of $40\mu A$, will be incident upon a 7-foil ^{12}C target with a total thickness of 700mg/cm^2, for a total elecron-nucleon luminosity of $\mathcal{L}_{eN} = 10^{38}\mathrm{cm}^{-2}\mathrm{s}^{-1}$. The scattered electron is measured in the Right-HRS magnetic spectrometer at an angle of 6° relative to the beam line with the use of a septum magnet, with a momentum of 2.4 GeV/c. The resulting virtual photon is produced at 4.3° on the left-side of the beam line. The K^- is detected nearby at 6° in the Left-HRS with a momentum of 2.7 GeV/c, again utilizing a septum magnet. The small angle between the photon and kaon minimizes the 4-momentum transfer t, emphasizing the t-channel diffractive processes; this also minimizes the 3-momentum transfer $\mathcal{Q}$ to the Θ^+, increasing the probability of forming a bound hyponuclear state. The Left-HRS will be equipped with threshold Čerenkov detectors to reject pions and electrons at the trigger level, and aid further in particle identification (PID) during the analysis. The Right-HRS will also use a gas threshold Čerenkov detector to reject pions at the trigger, and the electrons will identified during the analysis with the Čerenkov detector and shower detector.

3.1 Kinematic definitions

The reaction taking place involves six four-momenta:

$$k = (E, \vec{k}), \text{for the incident electron}$$

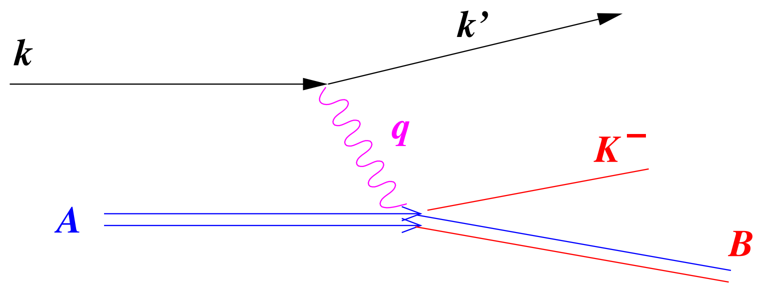

Figure 3: Kinematic variables for describing exclusive electron-nucleus scattering to a bound state: k and k' are the four momenta of the incoming and outgoing electrons, A and B are the four momentum of the target and bound final-state nuclei, and $q = k - k'$ is the four momentum of the exchanged photon.

$$\begin{aligned}
k' &= (E', \vec{k}'), \text{for the scattered electron} \\
N &= (M, \vec{P}), \text{for the target nucleon in the nucleus} \\
A &= (M_A, \vec{P_A}), \text{for the target nucleus} \\
K &= (E_K, \vec{p_K}), \text{for the final state kaon} \\
B &= (M_B, \vec{P_B}), \text{for the final state nucleus.}
\end{aligned}$$

In addition, it is useful to use

$$q = (k - k') = (\nu, \vec{q}), \text{for the virtual photon, and}$$

$$q^2 = \nu^2 - \vec{q}^2 = -Q^2.$$

Under the assumption of the exchange of a single virtual photon, the electro-production cross-section can be expressed as:

$$\frac{d\sigma^3_{\Theta^+}}{dE' d\Omega_e d\Omega_K} = \Gamma \frac{d\sigma_{\Theta^+}}{d\Omega_K}$$

with

$$\Gamma = \frac{\alpha}{2\pi^2} \frac{E'}{E} \frac{s - M^2}{MQ^2} \frac{1}{1-\epsilon} \tag{1}$$

$$\epsilon = \left(1 + 2\frac{|\vec{q}|^2}{Q^2} \tan^2 \frac{\theta_e}{2}\right)^{-1} . \tag{2}$$

Here Γ is the virtual photon flux, ϵ specifies the polarization of the virtual photon, $d\Omega_e$ and θ_e are the solid angle and scattering angle subtended by the scattered electron, and the Mandelstam variable $s = (q+N)^2$ is the invariant sum of the photon-nucleon four momentum. We will also use the Mandelstam variable $t = (q - K)^2$, the 4-momentum transfer to the nucleus, and $\mathcal{Q} = (\vec{q} - \vec{p_K})$ as the 3-momentum transfered to the nucleus.

4 Experimental Setup

The experiment will be performed in Hall A using existing equipment. The Left and Right High Momentum Spectrometers (L-HRS and R-HRS), when coupled to the septum magnets constructed for E94107, can access scattering angles of 6°. The particle identification capabilities of the spectrometers are also excellent in this momentum range through the use of Čerenkov detectors and time-of-flight measurements with resolutions better than 240ps over a 27m pathlength.

The configuration borrows from experience gained during the recently run Hall A Hypernuclear experiment E94-107, where Λ-hypernuclei were under study. However, due to the need to detect the negatively-charge kaon and the subsequent high rate of electrons in the spectrometer, the configuration has been re-optimized.

4.1 CEBAF Electron beam

The experiment as proposed would use a 5.75 GeV electron beam with a moderate beam current of 40μA with the standard 499 MHz frequency.

4.2 Target

The experiment will use the standard Hall A solid target ladder with a multi-foil ^{12}C target. The multi-foil carbon target will consist of seven 100mg/cm^2 foils, spaced 3cm apart and 5mm wide, providing a total thickness of 700mg/cm^2. This configuration will permit us to identify the foil for each reaction by each spectrometer independently, to help to reject accidental coincidences.

4.3 High Resolution Spectrometers

The L- and R-HRS's will be used to detect the K^- and scattered electron, respectively. The basic parameters for the spectrometers are given in Table 1. The moderate acceptances of the spectrometers will permit the collection of data over a range of hyponuclei masses simultaneously. With vacuum coupling to the scattering chamber and the good angular and momentum resolutions, we can achieve an instrumental resolution of 1 MeV.

Both HRS spectrometers will be instrumented with threshold Čerenkov PID detectors and shower detectors to aid in electron and hadron identification. Figure 4 presents the threshold momenta of different negative particles for the available Čerenkov radiators. The momentum region of the collected kaons is marked by the box centered at 2.67 GeV/c.

4.3.1 L-HRS Particle Identification

The L-HRS has a number of detectors to aid in particle identification. Two aerogel Čerenkov detectors, A1 and A2, with indices of refraction $n = 1.015$ and 1.055, respectively, were used in experiment E98-108 to separate K^+'s from π^+'s and protons. Their effectiveness can be seen in Figure 5. In the proposed experiment the rejection of pions and electrons in the L-HRS will be accomplished with the A1 Čerenkov detector and a time-of-flight (ToF) measurement. The aerogel Čerenkov detector A1 will be used on-line in the trigger to reject more than 90% of electrons and pions without reducing the kaon efficiency for particle momenta less than 2.84 GeV/c. In excluding electrons the pion-rejector (PR), a short two-layer shower detector, could be used to achieve another factor of 10 reduction in the accepted electron rate.

The standard HRS detector package includes two scintillator planes, S1 and S2, which are used in coincidence to form the base trigger. In 2003 the S2 trigger-planes in the L- and R-HRS were upgraded, increasing their segmentation and improving the timing resolution. The resulting new S2m detectors have intrinsic timing resolutions of 150ps, permitting a time-of-flight measurement using only the two HRS's with an achieved resolution better than 240 ps, as shown in Figure 6; this is more than sufficient to select events where the electron and hadron came from the same beam-bunch. The resolution could

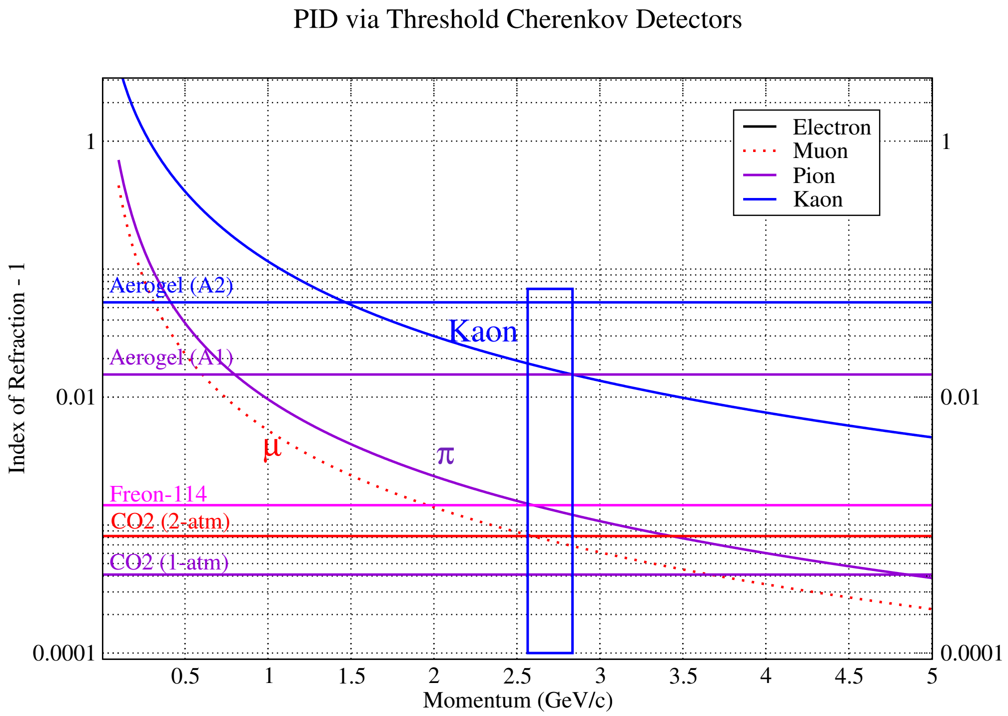

Figure 4: The indices of refraction for the different available Čerenkov detectors and the threshold momenta for K^-, π^-, and μ^- particles.

Central Momentum p_0 [GeV/c]	$0.3 - 4.3$ (L-HRS)
	$0.3 - 3.0$ (R-HRS)
Momentum acceptance $\Delta p/p$ [%]	± 4.5
Minimum Central angle θ_0	$6°$ with septum
In-plane angular coverage ϕ [mr]	30
Out-of-plane angular coverage θ [mr]	60
Transverse Length acceptance y [cm]	± 5
Solid angle at $\delta p/p = 0, y = 0$ [msr]	4.3
Momentum resolution σ_p/p	$1.1 \cdot 10^{-4}$
In-plane angular resolution (rms) [mr]	2.0
Out-of-plane angular resolution (rms) [mr]	1.5
Transverse position resolution σ_y [mm]	1.5
Trigger segmentation	16
Timing resolution $\sigma_{\rm ToF}$ (ps)	200

Table 1: Parameters describing the performance of the HRS spectrometers.

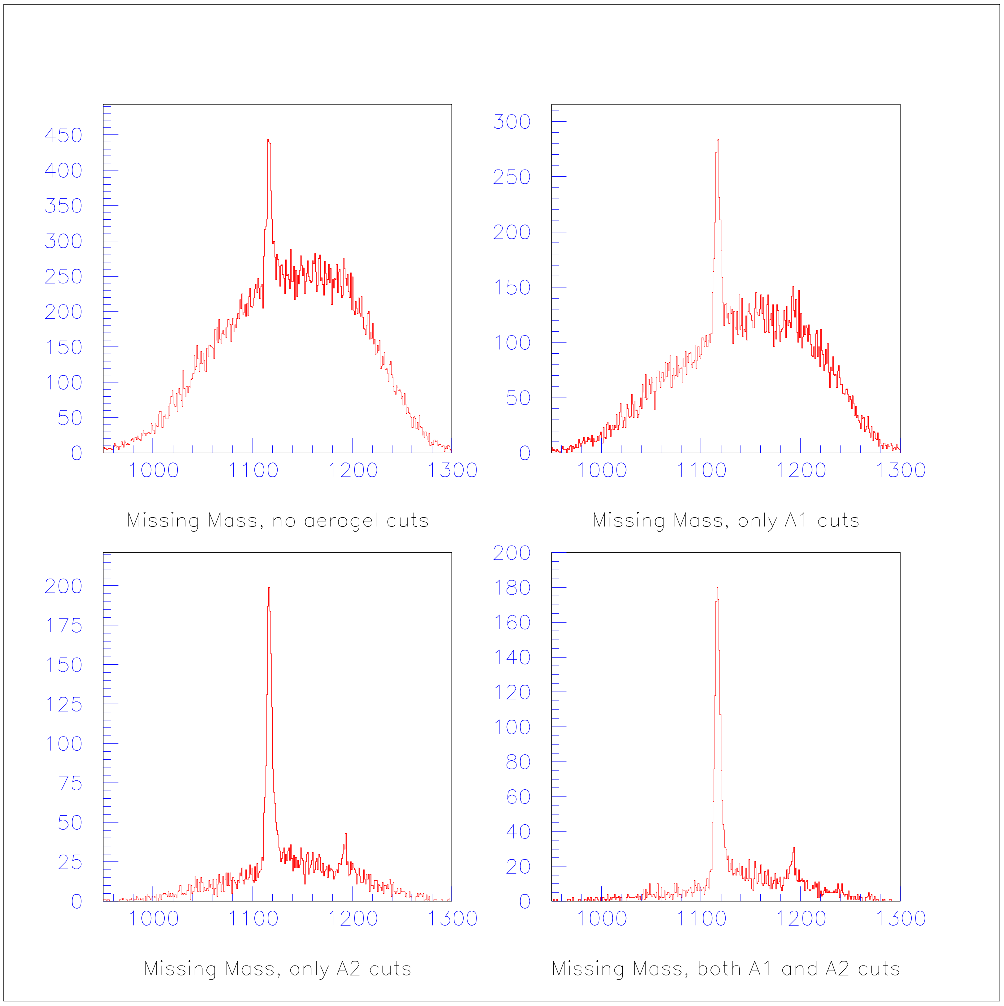

Figure 5: The missing mass spectra for the reaction $H(e, e'K^+)$ for different PID cuts on the aerogel detectors. The data is from E98-108.

be further improved through a comparison with the accelerator's RF signal. With a pathlength of 27 m from the target to S2m, the ToF for 2.7 GeV/c kaons and pions differ by 1.3ns, or more than $5\sigma_{\rm ToF}$.

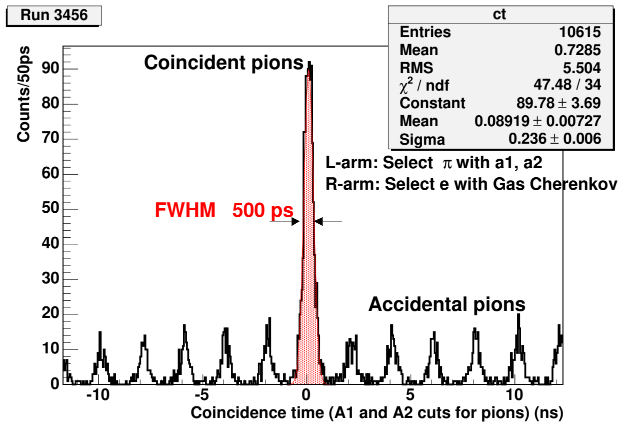

Figure 6: A time-of-flight measurement for 1.9 GeV/c pions. The data is from experiment E94-107 which ran in early 2004.

For E94-107, a Ř̌ing Ǐmaging Čherenkov (RICH) was used in addition to A1 and A2 to identify positive kaons. However, due to the high expected singles rates in the HRS (listed below), we do not plan to utilize this detector.

4.3.2 R-HRS Particle Identification

The R-HRS also has PID detectors to select electrons from pions. The standard CO_2 gas Čerenkov detector with $n = 1.0004$ has provided an on-line π^- rejection factor of 20, with factors of 200-300 obtained in off-line analysis. The preshower/shower electromagnetic calorimators on the R-HRS can provide an additional trigger-level pion rejection factor of 10, and 100-300 in off-line analysis. As with the L-HRS, the S2m scintillator plane with an intrinsic timing resolution of 150ps will be used to select coincident events from the same beam bunch.

4.4 Equipment Configuration

To maximize the production rate and the sticking probability λ, we need to maximize the virtual photon flux Γ and minimize the 3-momentum transfer to the nucleus, $\mathcal{Q}$. For this purpose, we plan to use the Hall A HRS with the two septum magnets in the 6 degree configuration.

This provides an angular acceptance of 4.3 msr and momentum acceptance of $\pm 4.5\%$ for observing both the electron and kaon.

The momentum settings were optimized, taking into account the kaon decay, the detected virtual photon flux, and minimizing the momentum transfer $\mathcal{Q}$. During the optimization the beam energy was constrained to be 5.75 GeV or less. The optimized momentum settings for the spectrometers were computed to be 2.41 GeV/c and 2.67 GeV/c for the Right and Left High Resolution Spectrometers, respectively.

4.5 Background Rates

In this section the expected DAQ trigger rates are estimated, as well as the rate of non-resonant true e^-K^- coincident events which form the background under the $^{12}_{\Theta}C$-production spectrum.

4.5.1 Single Rates

The singles rates for inclusive electroproduction reactions were estimated for a 40 μA, 5.75 GeV electron beam incident upon a 700mg/cm^2 ($\chi/\chi_o = 1.6\%$) carbon target, for a total electron-nucleon luminosity of $\mathcal{L}_{eN} = 10^{38}\text{cm}^{-2}\text{s}^{-1}$. The solid-angle for the HRS's was taken as 6 msr for the trigger rate estimation; the solid-angle for analysis-level background estimates was cut down to 4.5 msr. The electron rate was calculated in a Quark-Fragmentation (QFS) framework[22] for a beam energy of 6 GeV. When compared to an estimate with the product of the virtual photon flux and total deuteron γd hadronic cross-section[23] for the 5.75 GeV beam energy, the QFS rates were 15% higher and used in this estimate. The hadron rates were calculated using Wiser's parameterization of inclusive hadron-production experimental data[24]. The kaon and pion survival probabilities were computed for the central momentum with a 27 m pathlength to the S2 trigger plane in the HRS; the (kaon,pion) survival probabilibities for the L-HRS and R-HRS were calculated as (26%, 84%) and (23%, 82%), respectively. Table 2 presents the expected singles trigger-rates for both the HRS-Left and HRS-Right.

The total single trigger rates were checked against scaled trigger rates (to accomodate the virtual photon flux) observed with ^{12}C and BeO targets during the Pentaquark partner-search experiment E04-012 in 2004, and agreed to within 20%.

	P_0 [GeV/c]	e^- [kHz]	π^- [kHz]	K^- [kHz]	Total [kHz]	Scaled Exp. [kHz]
R-HRS	2.41	230	176	1.4	410	425
L-HRS	2.67	280	145	1.3	430	365

Table 2: The singles rates in the two spectrometers for different particle species at $\mathcal{L}_{eN} = 10^{38}\text{cm}^{-2}\text{s}^{-1}$.

4.5.2 Accidental Coincidence Rate

For the accidental coincidence rate calculation, a 50 ns coincidence time-window was assumed. An on-line rejection factor of 10 or better for pions and electrons in the K^--arm will be achieved through the use of the A1 Čerenkov detector. The R-HRS will be able to reject π^- from the electron sample by at least a factor of 20 on-line with the use of the gas Čerenkov detector. The breakdown of the accidental coincidence rates for an identified electron in the R-HRS and an electron, pion, or kaon in the L-HRS are given in Table 3. After including A1 as a veto in the trigger, the total rate of accidental coincidences that appear as candidate events is 507 Hz.

The contribution of e^-/e^- events could be further reduced from 322Hz to approximately 40Hz with the inclusion of the pion-rejector on the L-HRS as a veto in the trigger.

R-HRS/L-HRS	Rate	w/ on-line e^-/K^- PID
e^-/e^-	3.2 kHz	322 Hz
e^-/pi^-	1.7 kHz	170 Hz
e^-/K^-	15 Hz	15 Hz
Total	4.9 kHz	507 Hz

Table 3: Accidental coincidence rates for the conditions of Table 2.

In the off-line analysis, the accidental coincidences will be reduced further. By requiring the electron and hadron to originate within the same beam-bunch (within 2ns) and the same target foil (1 of 7), an additional suppression factor of 175 is gained. Off-line cuts on A1 should achieve an additional rejection factor of 10 for pions and and electrons, for a total rejection-factor of 100 from the detector. Finally, the time-of-flight measurement, in which the π^- and K^- flight-times differ by more than 5σ, will be used to clean up the event sample. The remaining accidental e^-K^- coincidences can be removed via the sideband-subtraction technique by purposefully selecting out-of-time kaons, though the uncertainty from statistical fluctuations of this background would remain.

4.5.3 True Coincidence Rates

At high beam energies the inclusive photo-production cross-section of hadrons can be understood within the framework of limiting fragmentation[25, 26]. In this approach, the invariant inclusive cross-sections $E\frac{d^3\sigma}{d^3p}$ are parameterized by the Feynman variable $x_F = p_{||}^{\mathrm{cm}}/p_{\mathrm{max}}^{\mathrm{cm}}$, and the perpendicular momentum of the hadron, $p_\perp$, relative to the photon direction. The inclusive cross-sections have been shown to be reasonably consistent with the limiting fragmentation hypothesis for photon energies as low as $E_\gamma = 3.2GeV$ at high x_F and low $p_\perp$[27, 28], the kinematic regime of this experiment. The $\gamma p \to \pi^-/K^-$ and $\gamma d \to \pi^-/K^-$ inclusive cross-sections have been compared for a photon energy of 18 GeV[29]; we observe the inclusive γd hadron-production cross-section tends to be simply a factor of two greater than the cross-sections for the γp initial state. For simplicity, the measurement of the $\gamma p \to \pi^-/K^-$ cross-section closest to the experiment's kinematics in [27] is used to estimate the $\gamma^* N \to K^-/\pi^-$ cross-section. The true-coincidence rates were then estimated using the virtual-photon flux factor (as determined by the beam and R-HRS) and the hadrons' photo-production cross-sections.

The pion and kaon kinematics, as determined by the L-HRS and the virtual photon, as well as the expected true-coincidence rates are presented in Table 4. The final rates take into account the losses due to particle decay. We find a 0.19 Hz e^-/K^- rate, which will be a non-resonant physics background underneath the desired ${}^{12}_{\Theta}C$ signal. This background is expected to have a smoother distribution across the missing-mass phase space than kaons from ${}^{12}_{\Theta}C$ production.

L-HRS PID	x_F	$p_\perp$ [GeV/c]	$E\frac{d^3\sigma}{d^3p}$ $[\mu b/GeV^2]$	Coinc. Rate [Hz]
π^-	> 0.78	0.23	29.9	66
K^-	> 0.93	0.23	0.225	0.19

Table 4: Rate of true-coincidences between an electron in the R-HRS and hadrons in the L-HRS.

$\sigma_{\gamma n}^{\Theta^+}$ shape	f_{γ^*,K^-}^{L-HRS}
Uniform in γn C.o.M.	0.0024
$\exp(3t)$ (selected)	0.033
$\exp(5t)$	0.052

Table 5: Values for the probability of the K^- being within the HRS's angular and momentum acceptance, given the electron is in the R-HRS, for different shapes of the Θ^+ production cross-section. The $\exp(3t)$-model with its acceptance of 0.033 is used in subsequent calculations.

5 Expected Results

In this section we calculate or estimate the factors that determine the rate of Θ^+-hyponuclei production. Among the most uncertain of these factors are the photo-production cross-section and the calculation of the "sticking factor" for the different neutron-Θ^+ transitions within the nucleus. Finally, we present an anticipated missing mass distribution for the ${}^{12}C(e,e'K^-){}^{12}_{\Theta}C$ final state.

5.1 Electroproduction of ${}^{12}_{\Theta}C$

The electroproduction rate of ${}^{12}_{\Theta}C$-hyponuclei at low Q^2can be expressed in terms of the product of the photo-production cross-section and the virtual photon-neutron luminonsity, $\mathcal{L}_{en}$. The effective photon-neutron luminosity is calculated as (see Section 3.1 for definitions):

$$\mathcal{L}_{\gamma^*\mathrm{n(eutron)}} = \frac{N}{A}(\Gamma\Delta\Omega_e\frac{\Delta E'}{E'}E')\mathcal{L}_{eN} \tag{3}$$

$$= \frac{6}{12}(1.15\cdot 10^{-5})(10^{38}/\mathrm{cm}^2/\mathrm{s}) = 5.75\cdot 10^{32}/\mathrm{cm}^2/\mathrm{s}. \tag{4}$$

(5)

The production rate for each ${}^{12}_{\Theta}C$ nuclear-state can be calculated separately. The states are annotated as $(nl_j^{-1}NL_J)$, where the state of the initial neutron, now a "hole"-state, and the Θ^+ are given by (nlj) and (NLJ), respectively. The rate for state $\mathcal{S}$ is:

$$\nu_{\mathcal{S}} = \mathcal{L}_{\gamma^* n}\cdot\sigma_{\gamma n}^{\Theta^+}\cdot f_{\gamma^*,K^-}^{L-HRS}\cdot f_K^{decay}\lambda_{\mathcal{S}} \tag{6}$$

where $\sigma_{\gamma n}^{\Theta^+}$ is the total Θ^+ photo-production cross-section from a neutron, $f_{\gamma^*,K^-}^{L-HRS}\approx 0.033$ is the acceptance factor for a K^- being detected in the L-HRS for a given γ^* and shape of the Θ^+ cross-section, $f_K^{decay}=0.27$ is the K^-'s survival probability for the 27m path to the S2 plane in the detector hut, and $\lambda_{\mathcal{S}}$ is the probability for a Θ^+ to bind to the nucleus in the state $\mathcal{S}$.

The f_{γ^*,K^-}^{L-HRS} and $\lambda_{\mathcal{S}}$ require additional explanation, and are covered in the next sections.

5.1.1 K^- acceptance calculation

The fraction of K^-'s which make it into the L-HRS's acceptance depend upon their distribution. As explained earlier, we expect diffractive processes to contribute strongly to the Θ^+ production mechanisms, and so expect a strong t-dependence to the cross-section in the forward direction, with $\sigma\propto\exp(Bt)$. This production channel is favored in models with a positive-parity Θ^+ [30]. To evaluate the acceptance, values of $B=0,3$, and $5\mathrm{GeV}^{-2}$ were used, and the results are shown in Table 5. For comparision, the slope parameter for the nearby $\Lambda(1520)$ is $B=6\mathrm{GeV}^{-2}$. In general for our kinematics, the K^- acceptance increases with larger values of B, due to the kaons being more tightly focussed along the virtual photon's direction. As a reasonable estimate, we used $B=3$ to calculation the acceptance factor.

To evaluate the acceptance, a simple Monte-Carlo for the L-HRS was written. The program used an R-function approach[31] which parameterized the results of a SNAKE-based model and analysis of the transport through the septa and spectrometers[32]. The acceptance calculation properly incorporated the correlations between the particle's momentum, point-of-origin, and direction at the target. In evaluating the acceptance, events were weighted by Γ and the t-distribution. The acceptance for settings from E04-012 were re-computed with this code as a check, and matched well.

5.2 Estimation of the "Sticking Probability" λ

To estimate the probability of forming a bound nuclear system from a Θ^+ and the residual nucleus, we looked to Λ-hypernuclei photoproduction as a guide. The process is schematically shown in Figure 7. Both reactions insert an "impurity" into the nucleus by exchanging a neutron (proton) with a Θ^+ (Λ); the impurity is not restricted by Pauli-blocking and therefore can populate any of its states. The distribution of the strange baryon amoung the states is governed by its momentum and the state of the initial nucleon.

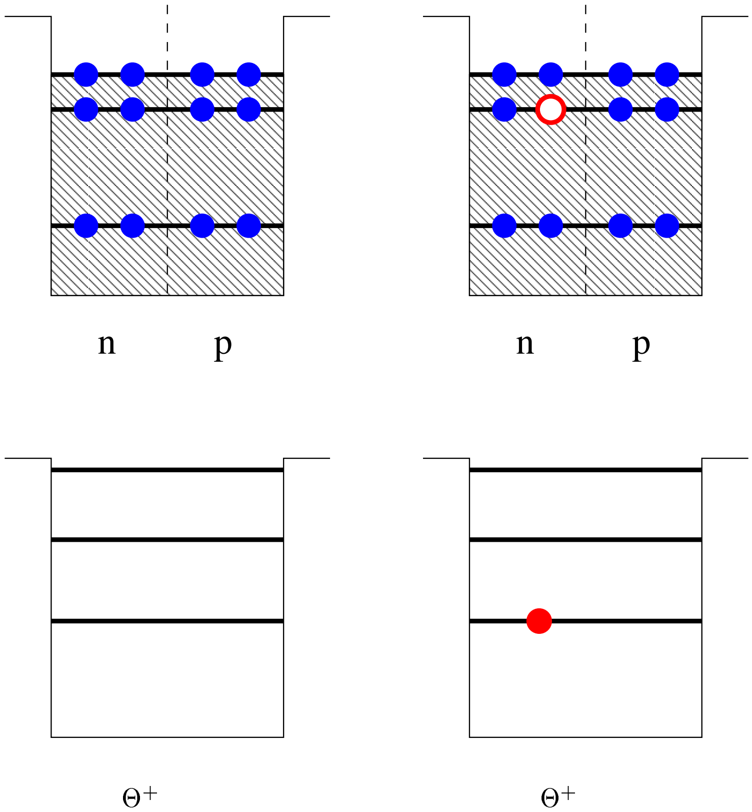

Figure 7: A neutron is replaced with a Θ^+-baryon in the nucleus.

Two approaches were used to finally estimate λ for specific Θ^+-hyponuclear states: a direct calculation and an empirical relation to similar Λ-hypernuclear states. The next section explains the general formalism surrounding λ for Λ-hypernuclei, followed by its application to Θ^+-hyponuclei.

5.3 Λ-hypernuclei Electroproduction

In the electroproduction of Λ-hypernuclei, the reaction is

$$e\_A \to e' K^+ B_\Lambda$$

where one of the protons in A has been exchanged for a Λ. The cross-section is calculated similarly as for photoproduction[33]:

$$\sum_f \frac{d\sigma^f}{d\Omega}(\gamma A \to K^+ B) = \mathrm{Z}\frac{d\sigma}{d\Omega}(\gamma p \to K^+\Lambda) \tag{7}$$

$$\sum_g \frac{d\sigma^g}{d\Omega}(\gamma A \to K^+ B_\Lambda) = \lambda \mathrm{Z}\frac{d\sigma}{d\Omega}(\gamma p \to K^+\Lambda) \tag{8}$$

where f denotes all final hypernuclear states (both bound and in the continuum), g only the bound final states, and Z the atomic number of the nucleus. However, generally the Λ is produced into the continuum; the probability for it to be bound to the nucleus is the "sticking probability", denoted here by λ. The probability for a particular nuclear transition, λ_S, can also be computed. Typical values for λ for Λ hypernuclei, summing over all hypernuclear states, are around 5% for $E_\gamma = 2$ GeV, where the depth of the binding potential for the hyperon is ≈ 30 MeV, as compared to a proton with a depth of 60 MeV[33]. As the momentum transfer to the nucleus increases, the sticking probability falls of rapidly. Figure 9 shows λ for the reaction $^{12}C(\gamma, K^+)^{12}B_\Lambda(1+; 1s^{-1}_{1/2}1s_{1/2})$ as extracted from [33], where a proton in the $1s_{1/2}$ state was substituted with a Λ in the same state.

To calculate the probability for a Λ being bound, one must compute the overlap of the initial nucleon's wave-function and that of the final-state hyperon. For zero-degree scattering ($\Lambda \equiv n_\Lambda l_\Lambda j_\Lambda$, $N \equiv n_N l_N j_N$) and based upon the formalism in [33], we find:

$$\begin{aligned} \lambda_{(N-1,\Lambda)} &\propto \left[C'(l_\Lambda\ l\ l_N, j_\Lambda\ j_B\ j_N)\ I_l\right]^2 && (9)\\ I_l &= \int_0^\infty u^*_\Lambda(r) j_l(qr) u_N(r) dr && (10)\end{aligned}$$

where C' is a product of Clebsh-Gordon coefficients, $j_l(x)$ is the spherical Bessel function, q is the magnitude of the 3-momentum transfer to the nucleus, and u_Λ/r and u_N/r are the single-particle radial wave functions.

In performing the calculation, we chose to use spherical harmonic-oscillator (SHO) wave-functions for u_Λ and u_N. The wave-functions are then of the form $u(r) = u'(\alpha r)$, where $b = 1/\alpha$ and is the oscillator parameter[34]. For ^{12}C and other $A = 12$ nuclei, the oscillator parameter that is typically used for nucleons is $b = 1.78$fm[33]. The solutions to the Schroedinger equation for the SHO have energies of:

$$E_{nl} = (2n + l + \frac{3}{2})\omega \tag{11}$$

where $\omega = \alpha^2/\mu$. By looking at the level-spacing, ω and therefore α were be determined for the Λ empirically. With a level spacing of 10MeV[33] for a Λ in ^{12}B, the oscillator parameter was assigned a value of $b_\Lambda = 1.96$fm.

For a comparison, we looked at the ratios of the differential cross-sections of specific hypernuclear states to those for the elementary $p(\gamma, K^+)\Lambda$ reaction; the cross-sections can be found in Figure 8. The effective sticking probability λ for a specific state could then be calculated according to 8 as the ratio of the hypernuclear and elementary production cross-sections. Since Q can also be directly calculated from E_γ, given the mass of the initial and final state particles, the dependence of λ on Q could be extracted. This is shown in Figure 9.

Using the SHO wave-functions for the u_Λ and u_N, we have computed the sticking probability for two transitions for the $^{12}C(\gamma, K^+)^{12}B_\Lambda$ reaction and compared the results with values extracted from [33],

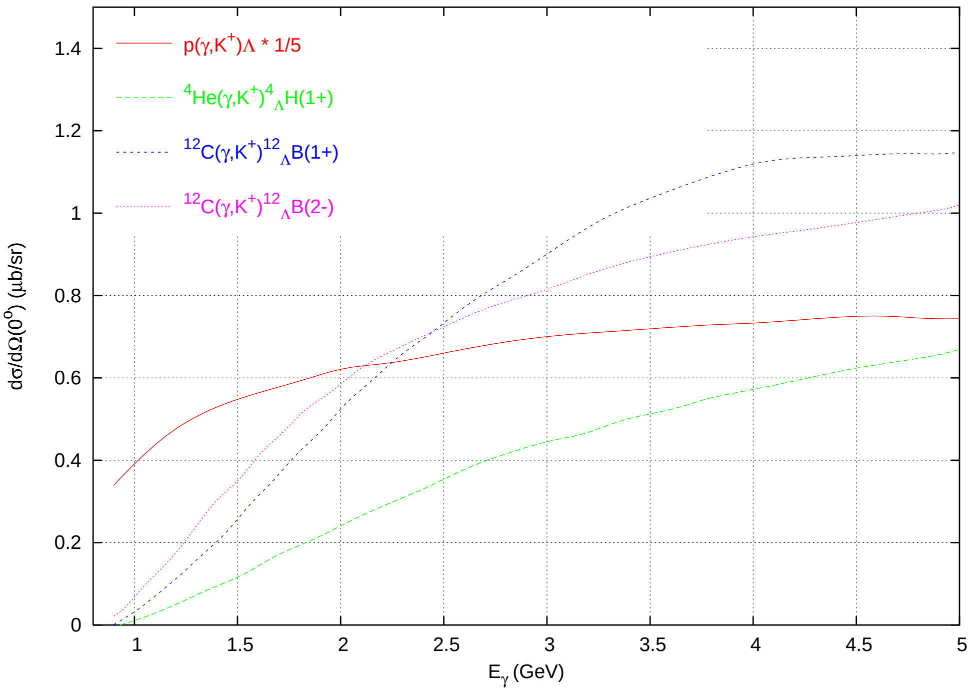

Figure 8: Calculations for the photo-production cross-sections of Λ production at $\Theta_{K\gamma} = 0°$. The elementary production off a proton (solid red) is scaled down by a factor of 5, for simpler comparison to the differential cross-sections for the specific hypernuclear states ${}^{4}_{\Lambda}H(1+; 1s^{-1}_{1/2}1s_{1/2})$ (dashed green), ${}^{12}_{\Lambda}B(1+; 1s^{-1}_{1/2}1s_{1/2})$ (short-dash blue), and ${}^{12}_{\Lambda}B(2-; 1p^{-1}_{3/2}1s_{1/2})$ (dotted purple)[33].

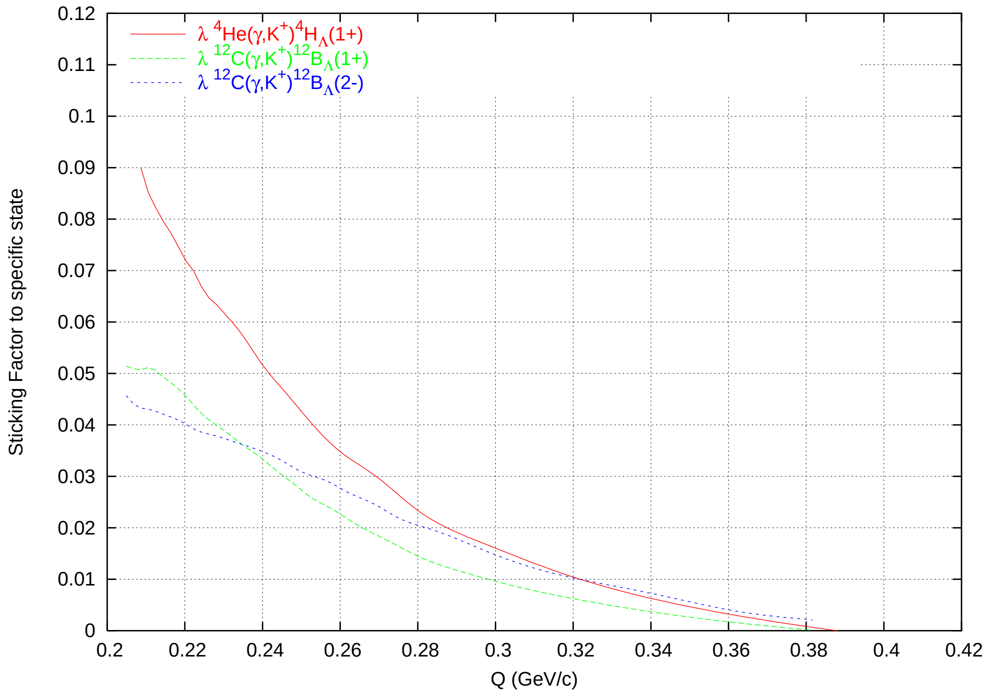

Figure 9: Extracted state-specific sticking factors λ versus the momentum transfer $\mathcal{Q}$. The hypernuclear states are ${}^{4}_{\Lambda}H(1+;1s^{-1}_{1/2}1s_{1/2})$ (solid red), ${}^{12}_{\Lambda}B(1+;1s^{-1}_{1/2}1s_{1/2})$ (dashed green), and ${}^{12}_{\Lambda}B(2-;1p^{-1}_{3/2}1s_{1/2})$ (short-dash blue).

as shown in Table 6. For the s-wave states, the match between the two calculations is a rather consistent factor of two, given the simplistic wave-function and model. However, for the proton in the p-wave we have a discrepancy which grows with increasing $\mathcal{Q}$, due to the poor match of the harmonic-oscillator potential near the edges of the well.

This factor of two will be used to "normalize" the calculation for the Θ^+ sticking probability below.

State	E_γ [MeV]	$\mathcal{Q}$ [MeV/c]	calculated λ	λ extracted from [33]
1+	2000	248	0.0167	0.028
	1200	331	0.0030	0.008

Table 6: Comparison of the calculations of λ for the ${}^{12}C(\gamma,K^+){}^{12}B_\Lambda(1+;1s^{-1}_{1/2}1s_{1/2})$ and ${}^{12}C(\gamma,K^+){}^{12}B_\Lambda(2-;1p^{-1}_{3/2}1s_{1/2})$ transitions.

5.4 Estimation of the "Sticking probability"

For the case of Θ^+K^- production, a similar relationship is assumed to hold, where the Θ^+ is produced off a neutron in the nucleus. Using the same form as (8), the photo-production cross-section for the Θ^+ is then:

$$\sigma_{B_{\Theta^+}} \equiv \sum_g \frac{d\sigma_{\Theta^+}}{d\Omega_K}(\gamma A \to K^- B^+_\Theta) = (\mathrm{A}-\mathrm{Z})\lambda_{\Theta^+}\frac{d\sigma_{\Theta^+}}{d\Omega_K}(\gamma n \to K^-\Theta^+) \tag{12}$$

To estimate λ for Θ^+-hyponuclei production, two approaches were taken.

5.4.1 Direct calculation

Using the same mathematical framework, we were able to calculate λ for the transition to the ${}^{12}_{\Theta}C$ final state. To determine b_{Θ^+}, the level spacings for the Θ^+ in carbon for the potential depths of 60 MeV and 120 MeV from [16] were used, leading to values of $b^{60}_{\Theta^+} = 1.39$fm and $b^{120}_{\Theta^+} = 1.06$fm, respectively. However, this calculation suffers from the same possible deficiency of the poor match near the cell wall. The effective sticking factor, summed over all the particle states, came out to be 2.2%; this is close to the nominal 5-10% seen in Λ-hypernuclei.

5.4.2 Equivalent Λ and Θ^+ momenta

We wish to relate the sticking factor for Λ-hypernuclear production to those for the Θ^+, taking advantage of the known kinematic dependence of the wave-functions. We assume the Λ and Θ^+ share the same form set of wave-function solutions within the nucleus, albeit with differing parameters to describe the depth of the potential and the particle masses.

We expect the momentum representation wave-functions to have the form:

$$\psi(p) = f(\beta p) = f(x)$$

where $x = \beta p$ is a dimensionless variable. In the non-relativistic and classical approach, $\beta \propto \sqrt{2\mu(E-V_0)}$ where μ is the reduced mass, V_0 is the depth of the potential, and $T_0 = E - V_0$ is the maximum kinetic energy of the state. This can be rewritten in more relativistic terms as:

$$\psi(p) = f'(T/T_0)$$

where T is the kinematic energy of the particle in the potential well.

With this relation, we can find an "equivalent" momentum transfer to relate the unknown values of $\lambda^+_\Theta(q)$ to the known $\lambda_\Lambda(q)$ (see Figure 9) for similar initial and final states. For a consistent set of potentials, we used [14] since the same group has successfully applied their quark mean-field model to conventional nuclei and Λ-hypernuclei[35, 36]. The potential depths at the standard nuclear density($\rho_0 = 0.145\text{fm}^{-3}$) were calculated as $V_0^{\Lambda} = -24\text{MeV}$ and $V_0^{\Theta^+} = -60\text{MeV}$. Since in $^{12}B_{\Lambda}$ nuclei the Λ in the ground-state is bound by $E = -12\text{MeV}$, we relate the kinetic energy of the Λ to that of the Θ^+ and look-up the sticking factor at the "equivalent" momentum. Figure 10 shows the ratio of the kinetic energy to the "critical" kinetic energy T_0 for comparing against the $j_B = 1^+ 1s^{-1}_{1/2} 1s_{1/2}$ transition in ^{12}C. The momentum transfer $\mathcal{Q}$ in these kinematics is between 650 and 700 MeV, with the Θ^+ kinetic energy between the $T_0 = (60-34)\text{MeV}$ (green) and $T_0 = 60\text{MeV}$ (blue) curves.

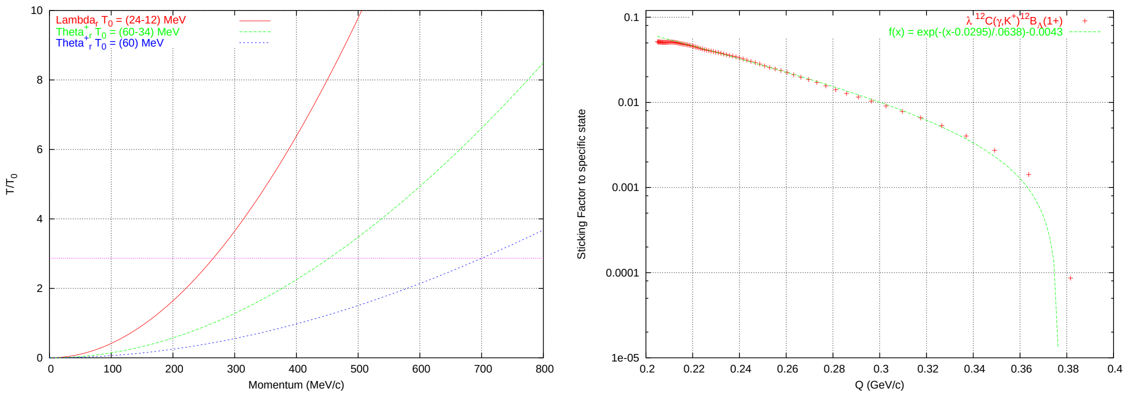

Figure 10: The left panel shows the correlation between the momentum and ratio of kinetic energies for the Λ and Θ^+. The right panel shows the λ for the Λ for the direct replacement of a proton in the $1s_{1/2}$ shell.

5.5 Expected Spectra

5.5.1 Monte Carlo

A number of inputs went into generating the anticipated distributions. The inclusive "true" $e - K^-$ physics-background and its distribution were determined from the parameterization of the experimental results in [29]. After comparing the results of [29] for γd to those in [27] for γp reactions, we found the cross-sections being used were too low by at least 40%. The random coincidence rate was uniformly distributed across the spectrometer focal planes.

The final missing-mass resolution was found to be near 0.7MeV from trials with the Hall A standard simulation MCEEP[37] where the beam energy spread, energy loss and multiple scattering from material around the target as well as at the VDCs in the spectrometer were taken into account. For the calculations here, the instrumental resolution was taken as 1 MeV. The width of the nuclear states were assigned a common value, under the assumption that the Θ^+'s natural width would dominate. The state widths and the photo-production cross-section were varied to explore the predicted spectra for different reasonable values of the parameters. Here, we define the missing-mass as the difference in binding-energy between Λ and nucleon, and it is given as:

$$M = M_{{}^{12}_{\Theta}C} - M_{\Theta} - M_{{}^{12}C} + M_n \tag{13}$$

where

$$M_{{}^{12}_{\Theta}C} = \sqrt{(k + A - k' - K)^2} \tag{14}$$

Using the 60 MeV deep potential of [16], Figures 11, 12, and 13 show the expected missing-mass distributions, and background level, for different trial total cross-sections and widths. The real physics background is shown in blue, with the accidental coincidence background shown in magenta. While we will subtract the accidental background in the analysis, using out-of-time events, the statistical uncertainties from the background will continue to affect the results.

The dominant challenge with the measurement for small binding energies is the level of the physics background. The excellent resolution of the HRS's provides a handle for separating the states from the background. For 200hrs of running time at $\mathcal{L} = 10^{38}/cm^2/s$, we will be able to identify and measure the dominant states listed here at the 6σ level for a total Θ^+ photoproduction cross-section of 10 nb.

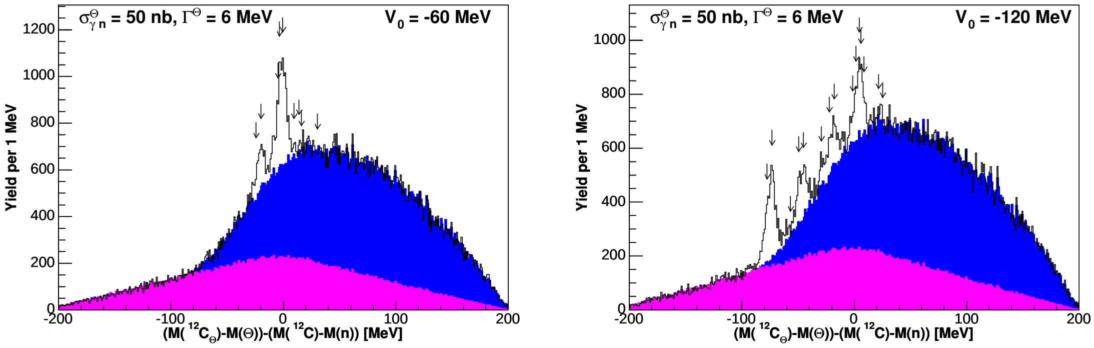

Figure 11: The expected ε_m spectrum after 200 hours of beam-time, assuming a value of $\sigma_{\gamma n}^{\Theta^+} = 50$nb and widths for the states of 6 MeV for a potential depth of 60 MeV (left) and 120 MeV (right).

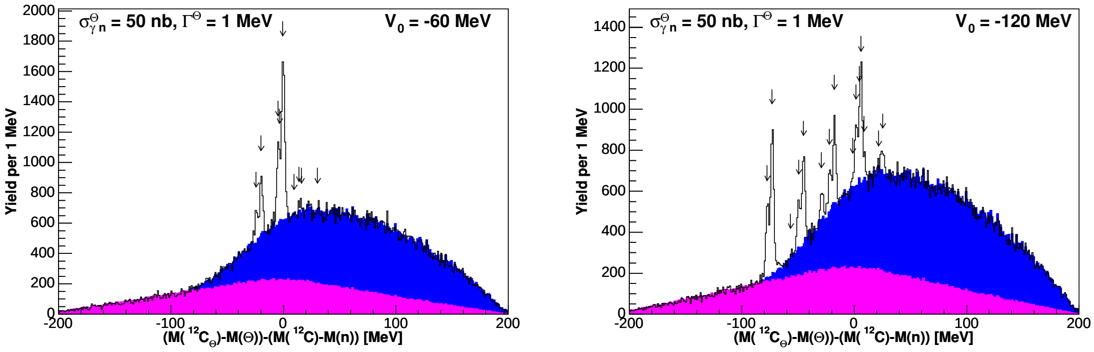

Figure 12: The expected ε_m spectrum after 200 hours of beam-time, assuming a value of $\sigma_{\gamma n}^{\Theta^+} = 50$nb and widths for the states of 1 MeV.

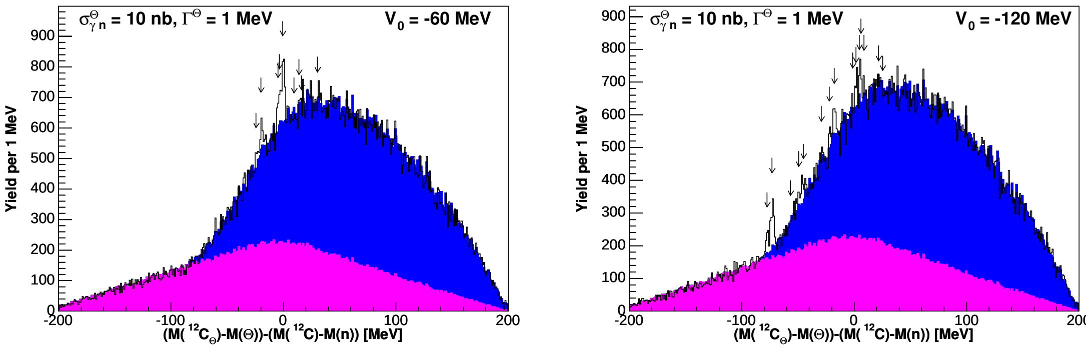

Figure 13: The expected ε_m spectrum after 200 hours of beam-time, assuming a value of $\sigma_{\gamma n}^{\Theta^+} = 10$nb and widths for the states of 1 MeV.

	current	energy	time
Type of measurement	[μA]	[GeV]	[hr]
HRS calibration	10	2.9	8
beam energy measurement	1	5.75	4
${}^{12}_{\Theta}C$ search	40	5.75	188
total			200

Table 7: The time allocation assuming 100% efficiency.

6 Summary of Expected Results and beam time request

The analysis presented here considered a minimum Θ^+ total photo-production cross-section of 10nb; for a cross-section significantly less than this the time required to collect adaquate statistics to overcome the large background becomes inhibitive.

6.1 Search for bound ${}^{12}_{\Theta}C$ states

The experiment will find the ${}^{12}_{\Theta}C$ bound states and measure their energy levels to 1 MeV. The intitial spin-orbit of the target neutron spreads the states by a few MeV, but the Θ^+ single particle states should be separated by tens of MeV. The determination of the absolute excitation energy will receive contributions from the knowledge of the beam energy ($2 \cdot 10^{-4} \times 5.75\text{GeV} = 1.2\text{MeV(FWHM)}$), the angles of the HRS to 1 mr and absolute momentum calibration to 1 MeV, leads to an uncertainty of about 1.3 MeV.

6.2 Beam time request

The purpose of the experiment is to search for bound ${}^{12}_{\Theta}C$ states, and measure their excitation energies. The experiment will be performed at only one kinematic setting, covering the entire range of interest, with a beam current of up to 40μA. Time is requested for calibration to properly ascertain the momentum and angular settings of the HRS's, as well as the beam energy. The experiment has been designed around the current maximum normally attainable beam energy of 5.75 GeV; if a 6 GeV or higher electron beam is reliably available, the experiment could benefit from its use with some minor changes to the spectrometer settings, and perhaps a change of the hadron-arm PID detectors.

References

[1] T. Nakano et al. *Phys. Rev. Lett.*, 91:012002, 2003. [LEPS Collaboration].

[2] S. Stepanyan et al. *Phys. Rev. Lett.*, 91:252001, 2003. [CLAS Collaboration].

[3] V. V. Barmin et al. *Phys. Atom. Nucl.*, 66:1715, 2003. [DIANA Collaboration].

[4] J. Barth et al. *Phys. Lett. B*, 572:127, 2003. [SAPHIR Collaboration].

[5] V. Kubarovsky et al. [CLAS Collaboration], arXiv:hep-ex/0311046.

[6] A. Airapetian et al. [HERMES Collaboration], arXiv:hep-ex/0312044.

[7] A. Aleev et al. [SVD Collaboration], arXiv:hep-ex/0401024.

[8] D. Diakonov, V. Petrov, and M.V. Polyakov. *Z. Phys. A*, 359:305, 1997.

[9] R.A. Arndt, Ya.I. Azimov, M.V. Polyakov, I.I. Strakovsky, and R.L. Workman. *Phys. Rev. C*, 69:035208, 2004.

[10] A. I. Titov, A. Hosaka, S. Date, and Y. Ohashi. Comment on the theta+ production at high energy. *Phys. Rev.*, C70:042202, 2004.

[11] Robert Jaffe and Frank Wilczek. arXiv:hep-ph/0401034.

[12] F. Csikor, Z. Fodor, S. D. Katz, and T. G. Kovacs. The status of pentaquark spectroscopy on the lattice. 2004.

[13] G. Miller. *Phys. Rev. C*, 70:022202(R), 2004.

[14] H. Shen and H. Toki. arXiv:nucl-th/0410072.

[15] X.H. Zhong, Y.H. Tan, L. Li, and P.Z. Ning. arXiv:nucl-th/0408046.

[16] D. Cabrera, Q.B. Li, V.K. Magas, E. Oset, and M.J. Vicente Vacas. arXiv:nucl-th/0407007.

[17] V.B. Kopeliovich and A.M. Shunderuk. arXiv:nucl-th/0409010.

[18] F. Garibaldi et al. High resolution hypernuclear 1p shell spectroscopy. Experiment E94-107, run at Jefferson Lab in 2004.

[19] Hyun-Chul Kim, Chang-Hwan Lee, and Hee-Jung Lee. Pentaquark theta+ mass and width in dense matter. 2004.

[20] H. Shen and H. Toki. Study of lambda hypernuclei in the quark mean field model. *Nucl. Phys.*, A707:469–476, 2002.

[21] H. Nagahiro, S. Hirenzaki, E. Oset, and M.J. Vicente Vacas. arXiv:nucl-th/0408002.

[22] Jr. J.W. Lightbody and J.S. O'Connell. Modeling single arm electron scattering and nucleon production from nuclei by gev electrons. *Computers in Physics*, page 57, May/June 1988.

[23] K. Hagiwara et al. Review of particle physics. *Phys. Rev.*, D66:010001, 2002.

[24] D. Wiser. *Ph.D. Thesis.* PhD thesis, University of Wisconsin, 1977.

[25] R. Feynmann. *PRL*, 23:1415, 1969.

[26] J. Benecke et al. *PR*, 188:2159, 1969.

[27] H. Burfeindt et al. Inclusive photoproduction of pions, kaons and protons at 6- gev. *Nucl. Phys.*, B74:189, 1974.

[28] H. Burfeindt et al. Measurement of inclusive photoproduction at 3.2 gev and comparison with electroproduction. *Phys. Lett.*, B43:345–348, 1973.

[29] A. Boyarski et al. Inclusive photoproduction of charged particles in the forward hemisphere. *Phys. Rev.*, D14:1733, 1976.

[30] M. Guidal, M.V. Polyakov, and M. Vanderhaeghen, November 6-8 2003. report from the Pentaquark workshop.

[31] V.L. Rvachev, T.I. Sheiko, V. Shapiro, and I. Tsukanov. On completeness of rfm solution structures. *Computational Mechanics*, 25:305–316, 2000.

[32] J. Lerose. private communications.

[33] Shian S. Hsiao and Stephen R. Cotanch. *Phys. Rev. C*, 28:1668, 1983.

[34] *Introduction to Quantum Mechanics.* Longman Scientific & Technical, 1989.

[35] H. Shen and H. Toki. *Nucl. Phys. A*, 707:469, 2002.

[36] H. Shen and H. Toki. *Phys. Rev. C*, 61:045205, 2000.

[37] "MCEEP — Monte Carlo for Electro-Nuclear Coincidence Experiments", User Manual, version 3.6, by P.E. Ulmer, Old Dominion University, unpublished (2001). Available from `http://www.physics.odu.edu/~ulmer/mceep/mceep.html`.